AAS 26-138

ADVANCING SPACECRAFT AUTONOMY FOR INTERPLANETARY TRANSFERS: OUTCOMES FROM THE EXTREMA PROJECT

Paolo Panicucci[*], Fabio Ornati[†], Eleonora Andreis[‡], Andrea Pizzetti[§] and Francesco Topputo[¶]

The increasing number of interplanetary spacecraft challenges the traditional reliance on the Deep-Space Network, which is costly and limited in capacity. The ERC-funded EXTREMA project pioneers a fully autonomous vision-based navigation (VBN) solution that allows spacecraft to determine their state using only planetary observations. This talk will showcase the validation and verification ecosystem developed to raise the VBN technology to TRL 3, including software-, model-, and hardware-in-the-loop simulations with real hardware and open-sky testing. This work presents insights into the navigation chain, testbed design and calibration, and outcomes that pave the way toward scalable autonomous deep-space missions.

INTRODUCTION

The space sector is undergoing a profound transformation driven by the rapid expansion of the new space economy, which is enabling an unprecedented number of deep-space missions.[1] The widespread adoption of CubeSats and small interplanetary probes has substantially lowered development costs and shortened development timelines compared to conventional spacecraft, effectively broadening access to space.[2,3] At the same time, this growth is placing severe pressure on ground-based navigation infrastructures such as the Deep Space Network (DSN) and ESTRACK. Current operational concepts rely primarily on radiometric tracking, which provides excellent accuracy, with position errors typically below the meter level and velocity errors on the order of millimeters per second.[4] However, this approach is costly and does not scale well with the increasing number of missions. These factors highlight the need for a paradigm shift toward spacecraft capable of autonomous Guidance, Navigation, and Control (GNC).[5]

Among the various solutions proposed to achieve autonomy, including X-ray pulsar navigation[6,7] and one-way radiometric techniques,[8,9] Vision-Based Navigation (VBN) has emerged as a particularly attractive option for small, resource-limited platforms. Although pulsar-based methods can achieve high accuracy even at astronomical distances,[10] they require large and power-hungry detectors that are incompatible with the constraints of miniaturized spacecraft. In contrast, VBN leverages compact, low-power optical sensors to measure line-of-sight (LoS) directions toward celestial

[*]Assistant Professor, Department of Aerospace Science and Technology, Politecnico di Milano, Via La Masa 34, 20156, Milan

[†]PhD Student, Department of Aerospace Science and Technology, Politecnico di Milano, Via La Masa 34, 20156, Milan

[‡]GNC Engineer, DLR, Robert-Hooke-Straße 7 28359 Bremen

[§]PhD Student, Department of Aerospace Science and Technology, Politecnico di Milano, Via La Masa 34, 20156, Milan

[¶]Full Professor, Department of Aerospace Science and Technology, Politecnico di Milano, Via La Masa 34, 20156, Milan

objects, enabling navigation without continuous ground support. A key advantage of VBN is its applicability across a wide range of mission phases, including interplanetary cruise,[11–14] medium-range operations,[15–17] and close-proximity or landing scenarios.[18–20] In deep-space applications, VBN typically processes images of unresolved bodies to extract centroids, which are converted into inertial directions using attitude knowledge and then fused within sequential estimators, commonly Extended Kalman Filters.[12,13,21,22] While this approach generally yields lower accuracy than radiometric tracking, with position uncertainties reaching several thousand kilometers during cruise, its flexibility, reduced operational cost, and maturity have made it the reference solution for autonomous navigation.

Despite significant theoretical progress, demonstrating operational robustness remains a major challenge. The validation and verification (V&V) of VBN algorithms are essential to close the gap between simulation and flight conditions,[23,24] particularly given the limited availability of representative deep-space image datasets. Software-in-the-loop simulations based on rendering engines provide an initial assessment but often neglect sensor-specific effects such as saturation, blooming, non-ideal noise, and electronic delays.[25,26] Consequently, comprehensive V&V campaigns must also address computational performance on representative hardware and assess algorithm robustness under realistic, non-Gaussian measurement conditions.

This paper presents the V&V framework developed within the EXTREMA project[27] to support reliable autonomous VBN in deep space. The proposed architecture combines a dedicated image-processing pipeline with a tightly coupled Extended Kalman Filter that directly exploits pixel-level measurements and accounts for effects such as light-time delay and relativistic aberration. A multilevel validation strategy is adopted, integrating high-fidelity software simulations with hardware-in-the-loop experiments using real optical sensors and onboard-class processors. The framework relies on a coherent rendering and optical stimulation chain designed to ensure both geometric and radiometric consistency.[28,29] Results for an Earth-to-Mars transfer demonstrate position errors below about 1,000 km and velocity errors under 0.5 m/s (3σ) in software-in-the-loop tests, with bounded performance degradation in hardware-in-the-loop conditions. Additional open-sky experiments further confirm the robustness of the image-processing chain under realistic environmental and sensing conditions, supporting the viability of VBN as a scalable alternative to ground-based deep-space navigation.

VALIDATION PHILOSOPHY

The V&V strategy adopted for the EXTREMA navigation framework is based on a progressive validation philosophy aimed at enabling a smooth transition of VBN algorithms from theoretical development to flight-representative deployment.

The validation process targets the two main components of a VBN system: the image processing (IP) chain and the navigation filter. The IP module extracts optical observables from raw camera images, such as planetary centroids or inertial LoSes.[13,21,22] These observables are then processed by the navigation filter to estimate the spacecraft state. Both components must ultimately operate on onboard processors with limited computational resources, meeting strict constraints in terms of execution time, memory usage, and latency.

Validating optical observable generation is particularly challenging due to the intrinsic complexity of imaging sensors. Cameras transform incoming light into digital images through a chain involving optics, detectors, and electronics, each introducing non-negligible distortions and noise sources.[30] Unlike scalar measurements, image-based observables rely on spatial correlations among pixels, meaning that any synthetic image generation must preserve both the geometric structure of the scene

and the underlying radiometric properties of light transport. This makes faithful image synthesis and emulation a critical and non-trivial aspect of VBN validation.
To address these challenges, the validation strategy follows an incremental approach with increasing realism. The process starts from idealized simulations in which the navigation filter is driven directly by synthetic measurements, bypassing the IP chain. It then progresses to high-fidelity simulations based on rendered images, enabling the assessment of IP robustness and the statistical properties of its outputs when interfaced with the filter. Finally, to account for unmodeled hardware effects and reduce the gap between synthetic and real data, hardware-in-the-loop testing is employed. In this setup, optical stimulators inject light into a real camera, whose images are processed end-to-end by the VBN pipeline. A key aspect of this approach is the co-design of the rendering engine and the optical stimulator, developed to ensure consistency between simulated scenes and physical stimulation, as discussed in Section Referencessec:codesign.
The overall verification roadmap is organized as a hierarchical pipeline to progressively increase the Technology Readiness Level (TRL):

- **Model-in-the-Loop (MIL):** Algorithm development and theoretical validation using numerical simulations with synthetic measurements and rendered images.
- **Software-in-the-Loop (SIL):** Implementation of the algorithms in flight-representative software to verify consistency with the MIL models.
- **Processor-in-the-Loop (PIL):** Execution of the compiled software on representative onboard processors to assess timing, latency, and memory constraints.
- **Hardware-in-the-Loop (HIL):** Integration of real optical sensors and processing hardware, stimulated by dynamically rendered scenes, to capture complex hardware effects such as saturation, blooming, electronic noise, and optical aberrations. A conceptual overview of the HIL setup is shown in Figure 1.

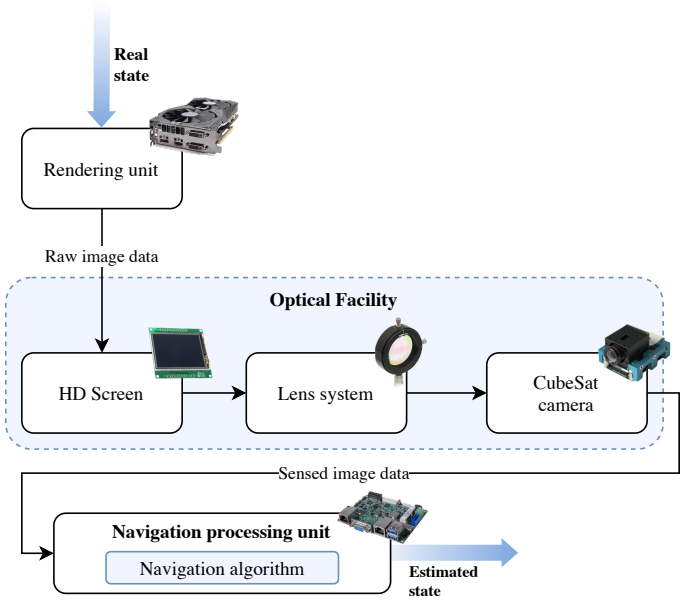

Figure 1: Functional sketch of the integrated HIL test (reproduced from[27]).

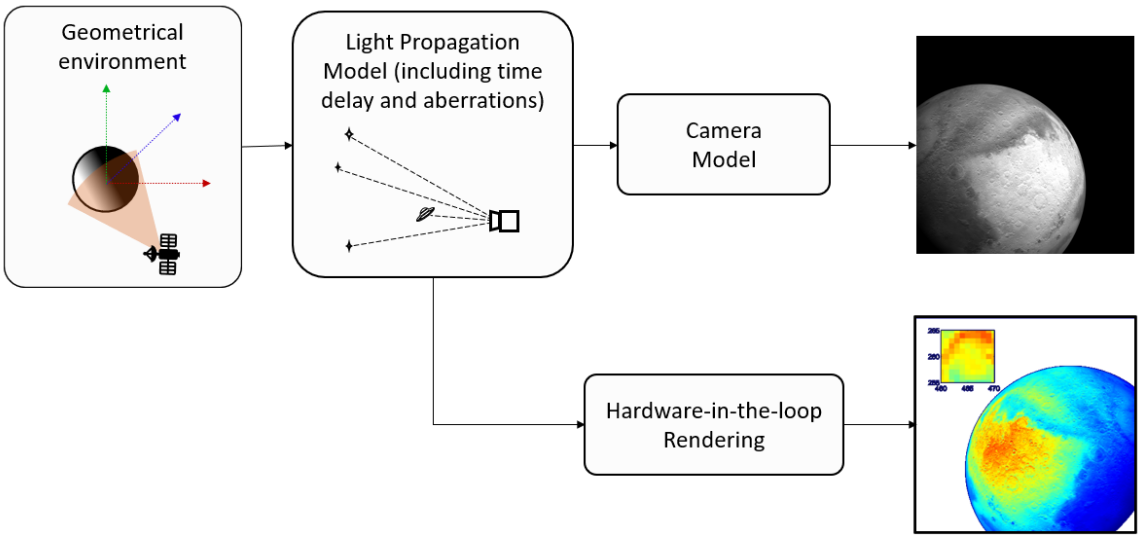

Figure 2: Functional block diagram of the renderer dual configuration

In addition to laboratory-based validation, the image processing chain was also evaluated through open-sky experiments in the Alpine region, allowing performance assessment using real celestial scenes without relying on the rendering engine.

HIGH-FIDELITY RENDERING ENGINE AND VALIDATION

Overview of the Rendering Tool

Accurate image reproduction is critical for validating autonomous VBN in deep space, where all celestial bodies appear unresolved as point-like sources. This differs from other navigation regimes, where bodies are spatially resolved and standard raytracing or rasterization tools are required.[30–33] To address the specific needs of deep-space navigation, a dedicated C++ rendering engine was developed. The engine operates as a TCP-server application orchestrating the SkySimulator, which handles both simulation logic and image visualization for HIL testing. A ”Dual Pipeline” configuration (see Figure 2) ensures consistent geometry computations while branching the final image formation according to the simulation mode: fully synthetic generation or HIL-compatible image output. Details on co-design with optical stimulators are provided in Section Referencessec:codesign.

Synthetic Generation

For software-based simulations (i.e., MIL, SIL, PIL), the engine functions as a high-fidelity digital twin of the flight camera, producing physically consistent synthetic images. Inputs include spacecraft trajectories from the SPESI simulator,[34] planetary ephemerides, and star catalogs (e.g., Hipparcos, Tycho) providing angular coordinates and photometric properties.[35,36] Planet and asteroid irradiances are computed using magnitude-phase laws.[37,38]
At each timestep, LoSes are computed from the spacecraft to celestial objects, and those outside the camera field of view are culled to reduce computation. Light-time delays[13,22] and relativistic aberrations[39] are applied before projecting the corrected LoSes onto the detector plane using a pinhole camera model with distortion. Radiometric calculations propagate irradiance through the optical

system and detector quantum efficiency to compute electron flux. A Gaussian point spread function (PSF) emulates optical aberrations, particularly critical for unresolved bodies, and the resulting electron counts are converted to digital numbers (DN) according to camera specifications. Figure 3 shows an example of a generated image.

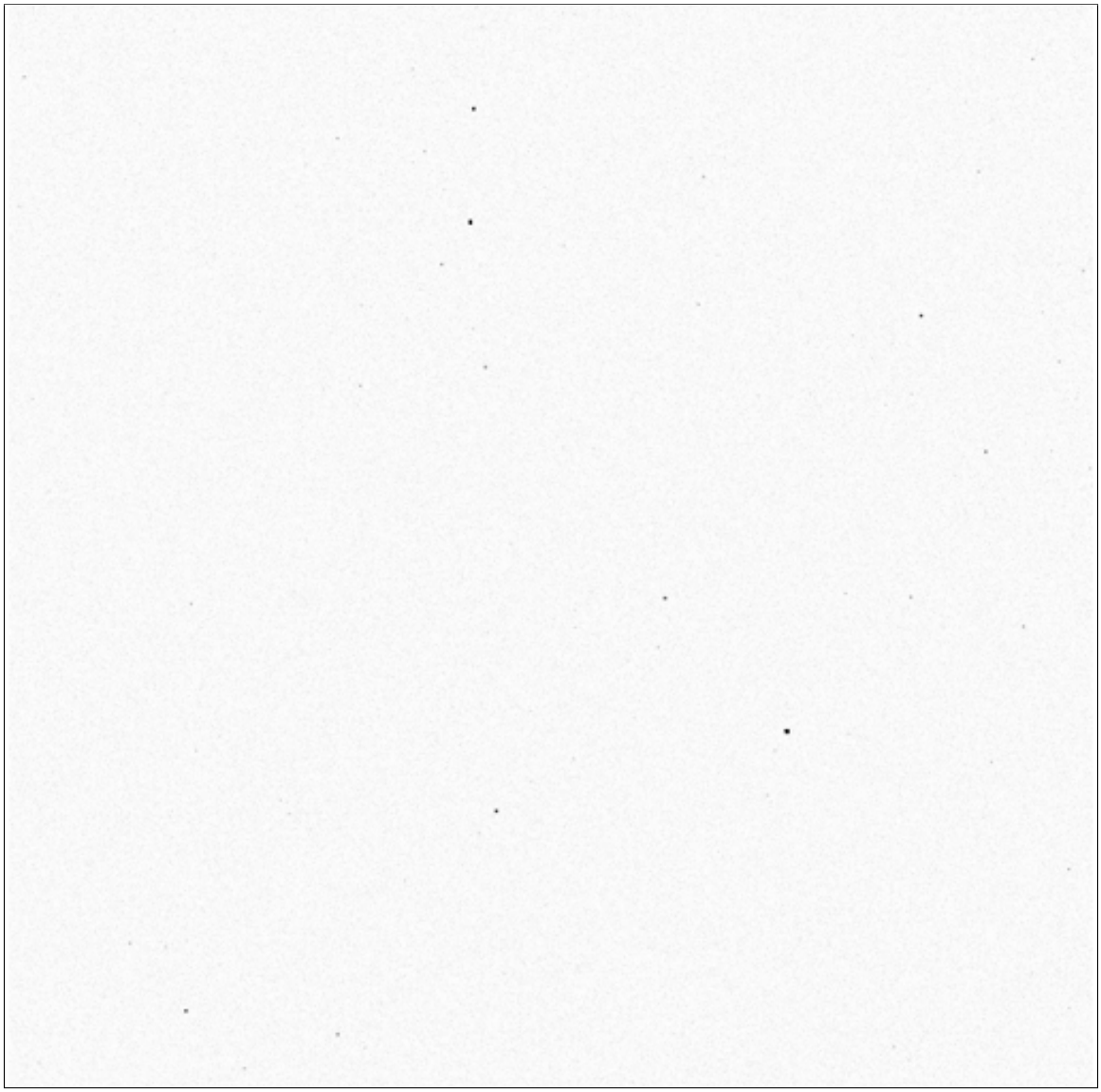

Figure 3: An image generated with the synthetic generation mode of the SkySimulator

Hardware-in-the-Loop Stimulation

For HIL simulations, the geometrical computation of LoSes is preserved, but image formation occurs on the real camera via an optical stimulator. Dedicated software compensates for geometric distortions and radiometric behaviors introduced by the stimulator to ensure consistency with orbital observations. Further details on these compensations are given in Sections Referencessec:codesign

and Referencessec:hilsetup.

Rendering Capabilities and Validation

The engine achieves real-time rendering at approximately 100 Hz, sufficient to operate alongside GNC algorithms without bottlenecks, even with complex star fields and multiple planetary bodies. Validation of the synthetic generation mode[40] was performed using Rosetta mission data,[41] modeling the NavCam.[42] Comparisons demonstrated subpixel geometric accuracy and radiometric precision, with RMSE of pixel intensities below the sensor noise floor. Open-sky experiments in the Alpine region further confirmed the consistency and reliability of the renderer for synthetic image generation.

DEEP-SPACE VISION-BASED NAVIGATION

Fundamentals of Celestial Triangulation

Celestial triangulation for deep-space navigation estimates the spacecraft's position by observing the LoS directions to known celestial bodies. This is a resection problem where the observer's location is inferred from angles to at least two known points.[14,43] If a spacecraft can measure LoS vectors to at least two celestial beacons simultaneously, it can instantaneously determine its position vector. The achievable accuracy depends strongly on the observation geometry. The triangulation problem becomes singular when the spacecraft and beacons are collinear, as no information is available along the LoS. It is worth noting that optimal beacon selection can improve position accuracy by identifying the most suitable planet to observe among available targets.[43] Moreover, operational constraints, such as spacecraft pointing limitations (e.g., avoiding the Sun) and sensor performance (e.g., limiting magnitude), might also be considered.
Altough asteroids have been already used in missions such as Deep Space 1,[11] CubeSats' limited optical sensor performance makes detecting faint minor bodies challenging. Therefore, planets are the preferred targets, as they are brighter and have well-known ephemerides.[44] These characteristics enable reliable identification with COTS sensors and reducing uncertainty propagation to spacecraft position. Yet, a key limitation is that simultaneous planet observations are often impossible due to the limited number of onboard cameras and their placement, making static triangulation only partially applicable in practice. To overcome this limitation, a filtering strategy allows asynchronous observation of multiple planets and recover the spacecraft position with dynamical linking.

High-Level Description of the EXTREMA Vision-Based Navigation

Given the impossibility of simultaneous tracking, a navigation filter is employed to correlate asynchronous measurements with spacecraft dynamics. The proposed concept of operations (ConOps) follows a repetitive navigation cycle with four sequential phases:[13]

1. The spacecraft orients to track the first selected planet for a fixed duration (typically 60 minutes), acquiring images at a defined frequency (every 100 seconds in this work).

2. The spacecraft performs a slew maneuver to reorient toward a second target planet. During the slew, no optical measurements are taken, and the filter performs only the propagation step. Slew duration is approximately 20–30 minutes but may vary with platform agility.

3. The spacecraft tracks the second planet for another 60-minute window.

4. The system enters a long propagation phase (5 to 10 days) during which the spacecraft does not acquire navigation measurements but propagates its state estimate using the dynamical model. This phase incorporates other spacecraft activities (e.g., thrusting, wheel desaturation).

This cycle maintains resource efficiency, dedicating only a small fraction of mission time (about 2.5 hours every 10 days) to active navigation. Planet selection follows the optimal beacon selection algorithm.[43]

The VBN strategy is a tightly coupled navigation algorithm integrating a robust IP pipeline with an efficient navigation filter. The IP provides pixel coordinates to the navigation filter, which then estimates the spacecraft position and other state variables over time. Implementation improvements from previous versions[13,21,45] focus primarily on computational efficiency during deployment iterations.

The IP pipeline operates in three stages: centroid extraction, attitude determination, and planet identification. Centroid extraction removes background noise and identifies connected pixel regions using a high-efficiency region-growing algorithm. A constant threshold is applied for computational efficiency, with sub-pixel precision obtained via the square of pixel intensities as weights.[46]

Attitude determination provides the spacecraft's inertial attitude, feeding the onboard attitude determination filter. The pyramid algorithm[47] matches star asterisms to a catalog. The proposed algorithm is bulked within a RANSAC framework to ensure robust attitude estimation. As a byproduct of this step, spikes (i.e., centroid not registered as stars) are identified, among which the target planet may be found.

Planet identification compares spikes to the expected planet location as computed from a priori trajectory information as obtained from the filter. Based on statistical consideration exploiting the planet expected position and its covariance, the spike with highest is registered as the planet.

The navigation filter uses raw planet pixel coordinates to estimate the spacecraft state under dynamics constraints. A 17-element continuous-discrete EKF state vector includes position, velocity, mass, and three sets of first-order Gauss-Markov (FOGM) processes for unmodeled accelerations, thrust errors, and camera calibration errors.

The filter has low-thrust and ballistic modes, depending on the spacecraft mode. Propagation uses a fourth-order Runge-Kutta scheme with continuous-time Riccati integration, including gravitational effects from the Sun and planets, and SRP. Thrust-dependent FOGM processes are converted from body to inertial frames for correct propagation.

The measurement update uses a tightly coupled pinhole camera model with analytical derivatives. Attitude uncertainty is incorporated by enalrging the pixel measurement covariance. Light-time delay and relativistic aberration are corrected analytically, avoiding iterative Newton-Raphson methods, reducing computational time by orders of magnitude.[13] Outliers are removed via measurement editing, and specialized FOGM absorbs sensor-dependent systematic errors. The update step is only performed during coasting, as measurements are not acquired during thrusting.

Summary of Numerical Results

MIL validation on a Earth-Mars transfer scenario combines standalone IP/filter testing and integrated assessments. Centroid determination achieves better than 0.3 pixels (3σ) accuracy, while attitude determination is 15 arcseconds. RANSAC succeeds in over 98% of scenarios, proving high

robustness. As Figure 4 shows, planet identification remains accurate to 0.3 pixels (3σ).

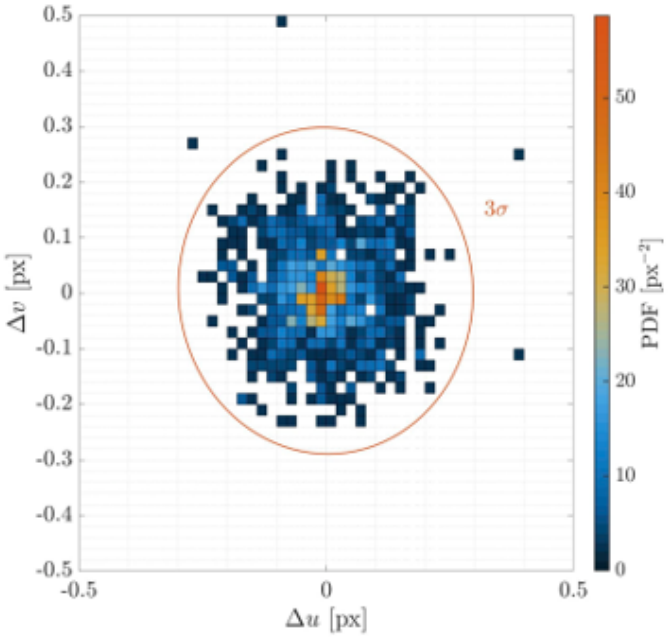

Figure 4: A 2D probability density function of the planet identification error.

First the filter has been tested with perfect LoSes, yielding position and velocity covariance bounds of 360 km and 0.04 m/s (3σ), respectivelly. Then the IP has been introduced in the simulation loop and the dynamical mismatch between the filter and the environment has been improved, MIL simulations obtained 3200 km and 0.8 m/s (3σ) for position and velocity covariance bounds (see Figures 5a and 5b). Results underlined the feasibility of the proposed navigation strategy for deep-space operations.

OVERVIEW OF THE HARDWARE-IN-THE-LOOP SETUP

Optical Stimulators

HIL simulations are a crucial step for validating deep-space VBN algorithms, enabling the use of real cameras to capture images under controlled conditions. Optical stimulators provide a cost-effective method for this validation by stimulating the camera sensor through collimated light from a screen displaying synthetic scenes. This allows the simulation to naturally include hardware-specific effects such as lens distortions, detector noise, saturation, and blooming. The optical stimulator therefore complements software-only simulations, ensuring the VBN pipeline is tested against the physical behaviors it will encounter in flight.

Optical stimulators can adopt single-lens or two-lens configurations. Single-lens setups are simple but fixed in magnification, while two-lens configurations allow variable magnification but require careful optical design to minimize distortions and aberrations (e.g., see 28, 29, 48, 49) . Figures 6a and 6b illustrate examples of both types of stimulators. For EXTREMA, dedicated attention has been put in optimizing the stimulator design in order to avoid blurring and aberration during the stimulation process. The resulting design has proven superior stimulation capability even at high

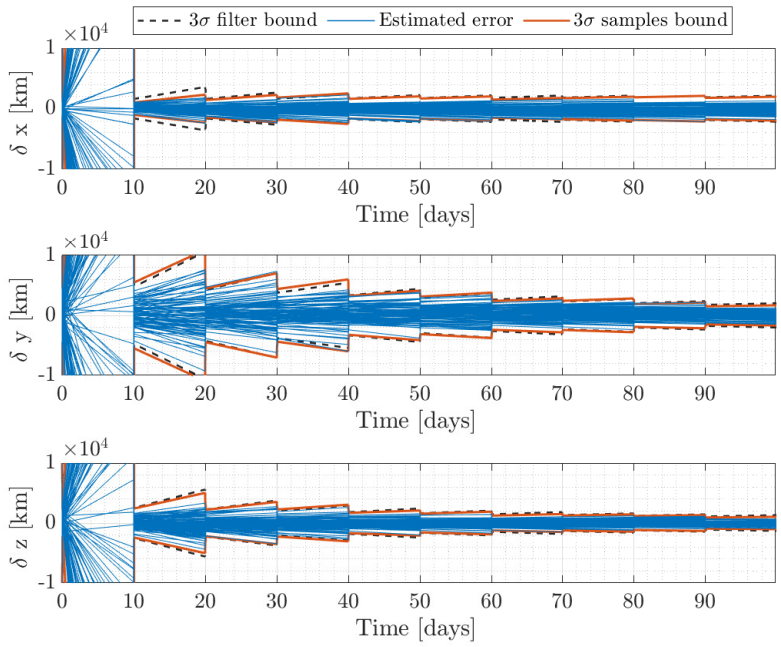

(a) Position

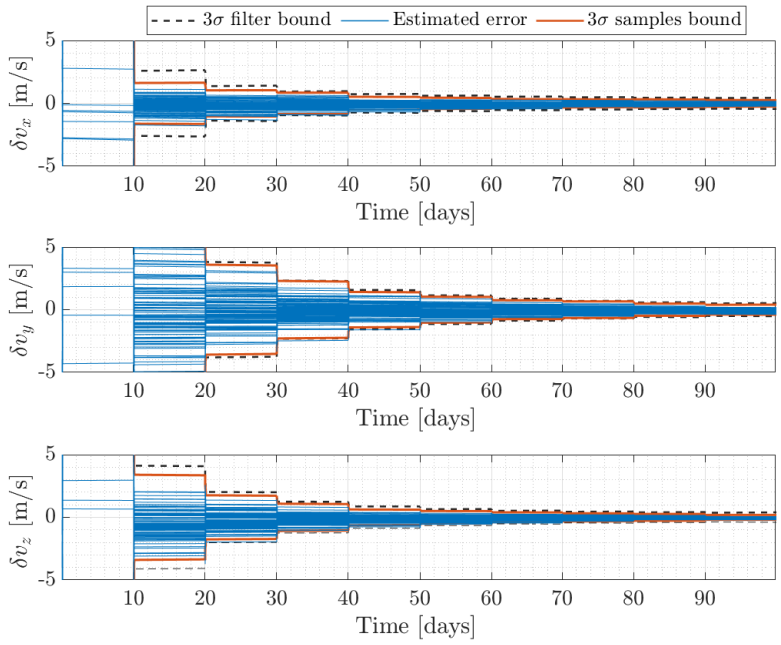

(b) Velocity

Figure 5: Estimated errors for each inertial Cartesian component with 3σ bounds.

angle with respect to the camera boresight, leading to subpixel accuracy in the stimulation over the entire image plane. More details can be found in 29.

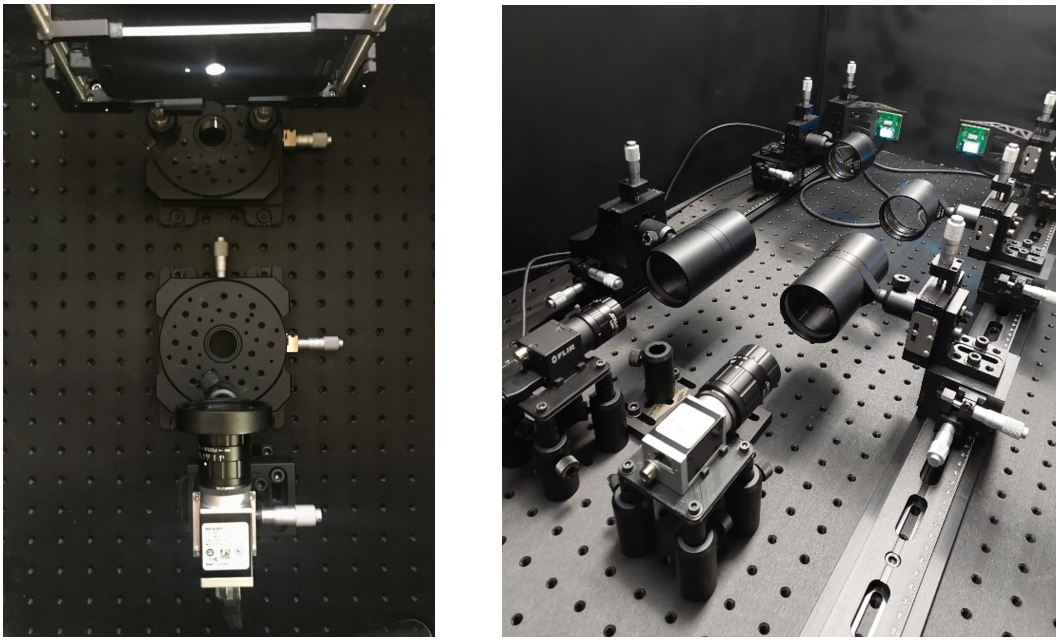

(a) Single lens configuration (b) Two-lens configuration

Figure 6: Example of optical stimulators.

Deep Space Geometric and Radiometric Calibrations

To achieve high-fidelity HIL stimulation, the facility must undergo accurate geometric and radiometric calibrations. On the one hand, radiometric calibration maps the screen pixel values to the correct light intensity at the camera pupil, ensuring the detector receives the correct photon flux for each celestial object. The calibration map is obtained by observing known pattern of increasing intensity to find the correlation between screen DN and light received at the camera pupil. On the other hand, geometric calibration corrects residual optical distortions and misalignments in the facility, so that the camera observes the scene as it would in orbit. Patterns of pointwise dots covering the field of view (see Figure 7) are used to determine a polynomial distortion model.

Facility-Renderer Integrated Design

Once facility calibration are available, the rendering engine exploits them to produce images that account for both radiometric and geometric consistency. In essence, the HIL stimulation mode of the renderer warps the celestial objects' positions to compensate for facility distortions and converts the virtual scene intensity to screen pixel values using the radiometric calibration curve. This ensures that the camera observes an image free of facility-induced distortions and receives the correct photon flux, producing realistic camera DN for VBN testing. The integration is schematically shown in Figure 8.

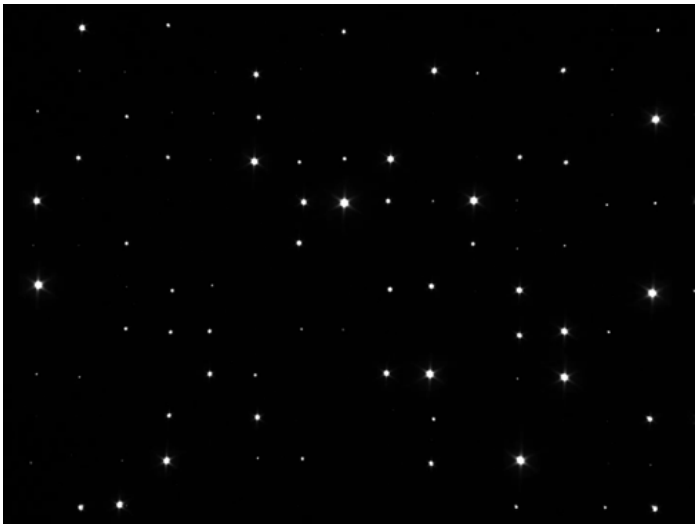

Figure 7: Example of geometrical calibration pattern.

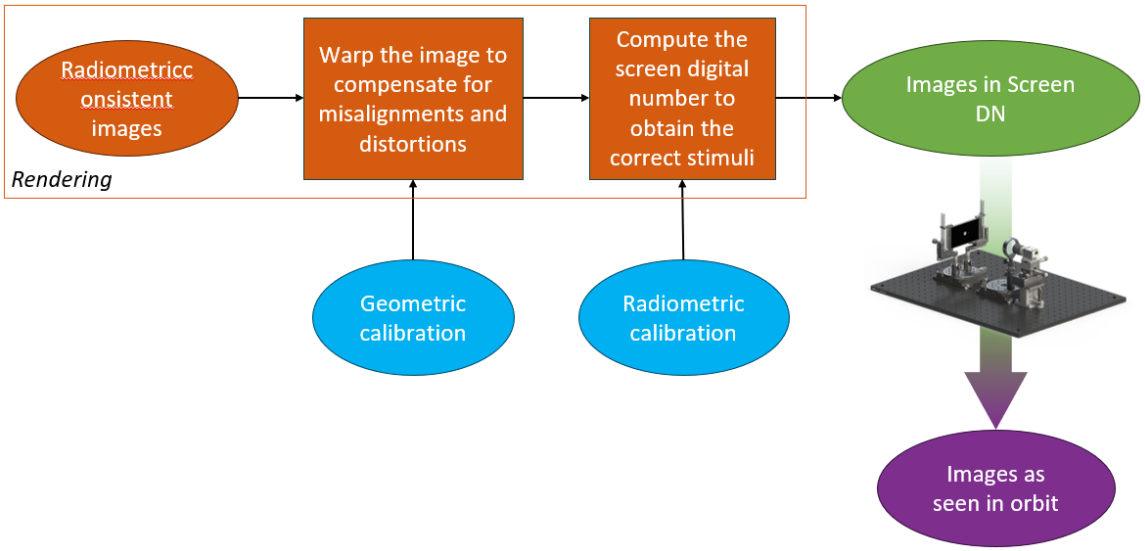

Figure 8: The block diagram of the HIL stimulation mode integrating the rendering and the optical stimulator

Validation of the Integrated Framework

The integrated HIL framework has been validated for both geometric and radiometric fidelity. Geometric calibration ensures residual angular errors are minimized, with the majority of measurements below 5–10 arcseconds (see Figure 9). Radiometric validation compared synthetic renderings with physical stimulations of Lambertian disks and night-sky observations using the RETINA facility. The facility reproduces predicted intensity profiles and stellar centroid positions with high accuracy as reported in 26. An integrated test involving geometric and radiometric compensation has been developed to reproduce night-sky observations. These tests of unresolved objects, such as Jupiter and the Pleiades, confirm that the framework faithfully reproduces both geometric and

radiometric characteristics of the scene (see Figures 10a and 10b).

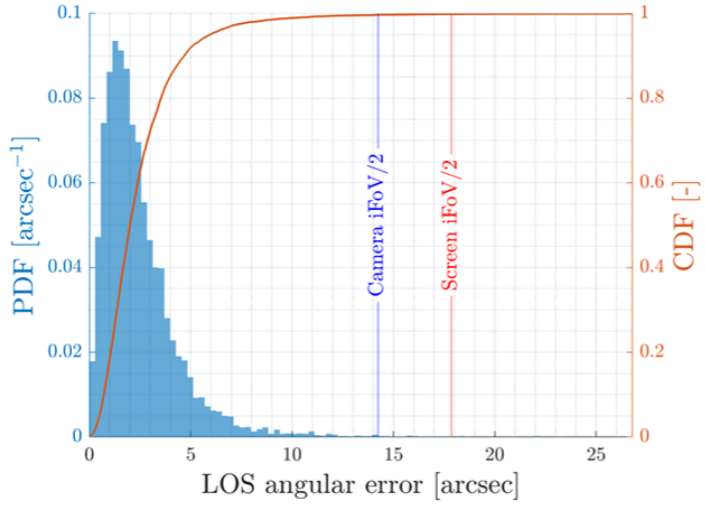

Figure 9: Angular errror statistics of the geometric compensation.

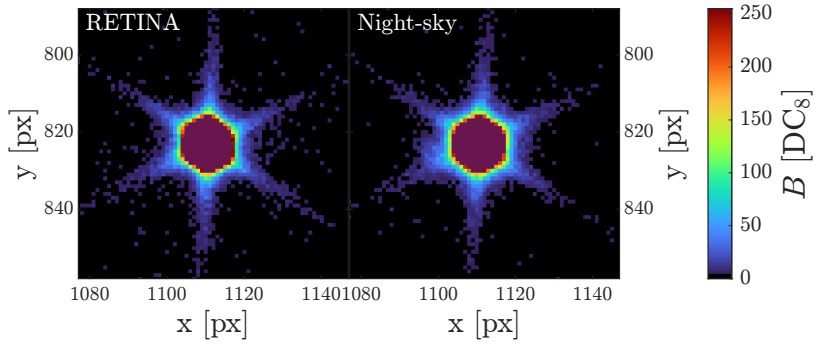

(a) Jupiter

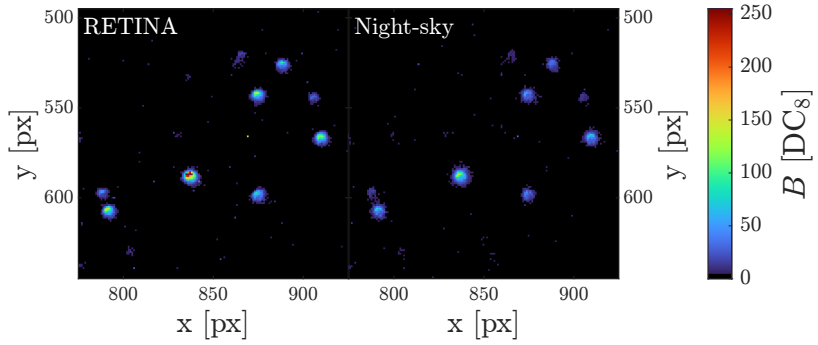

(b) Pleiades

Figure 10: Comparison between night-sky and RETINA acquisitions for unresolved objects (taken from[26]).

HARDWARE-IN-THE-LOOP VALIDATION CAMPAIGN

The HIL validation campaign was conducted to evaluate the performance of the deep-space VBN algorithm under realistic conditions, bridging the gap between synthetic simulations and flight-like operations. The tests were performed using the RETINA optical stimulator, with calibrated geometric and radiometric settings, and images were acquired by a COTS camera. The acquired images were then processed by the VBN algorithm running on a representative onboard processor, a ZynqUltrascale+ SoC ARM Cortex-A53 1.2 GHz.

The integrated HIL experiments confirmed the robustness of the VBN pipeline in the presence of unmodeled errors such as residual calibration misalignments, lens distortions, non-ideal PSFs, and sensor-specific artifacts. The IP pipeline successfully determined spacecraft attitude and extracted planet LoS measurements from the physical images with performance comparable to MIL simulations.

Monte Carlo results from the HIL navigation campaign show an expected degradation in navigation accuracy compared to idealized SIL simulations, reflecting the "reality gap" introduced by hardware effects. Steady-state $3(\sigma)$ position errors ranged from approximately 5,320 km to 5,491 km, while $3(\sigma)$ velocity errors were between 0.97 m/s and 1.23 m/s (see Figures 11a and **??**). A more detailed investigation revealed that these errors are primarily driven by the finite resolution of the display pixels and residual uncertainties in the facility calibration. Despite this degradation, the VBN algorithm remained consistent and capable of autonomously estimating the spacecraft state within acceptable bounds for deep-space cruise, demonstrating robustness against unmodeled effects present in the physical test environment. Computational performance of the fully integrated VBN algorithm was assessed on the ZynqUltrascale+ SoC. The complete pipeline executed in under 40 ms, confirming real-time capability on space-representative hardware. The runtime distribution demonstrates that centroid extraction, attitude and planet identification, filter propagation, and filter update are all executable within the timing constraints required for autonomous deep-space navigation.

Finally, open-sky validation campaigns were also performed to further verify the IP chain under real observational conditions. Images of unresolved celestial bodies were acquired in northern Italy and compared with facility-stimulated images (see Figure 12a and 12b). These tests confirmed that the VBN algorithm can accurately detect planets and stars, including faint targets like Uranus, while maintaining attitude determination and LoS extraction performance.

CONCLUSIONS

The rapid increase in interplanetary missions is putting a growing strain on ground-based infrastructure, creating an urgent need for autonomous spacecraft capable of determining their own trajectory onboard. This work presents the design and validation of a vision-based navigation (VBN) algorithm tailored for deep-space CubeSats. The solution integrates a robust image processing pipeline with an extended Kalman filter that directly processes pixel-level measurements of planets. The algorithm was validated through a HIL campaign using a calibrated optical stimulator and a high-fidelity rendering engine. The HIL setup ensured that the camera received realistic visual input representative of deep-space conditions. Geometric calibration achieved sub-pixel stimulation accuracy with angular errors below 10 arcseconds, while radiometric fidelity was confirmed through comparisons with real night-sky observations, achieving high structural similarity in all tests.

The validation campaign progressed directly to fully integrated HIL experiments. The final experiment combined the calibrated optical stimulator, renderer, and a physical camera with the VBN

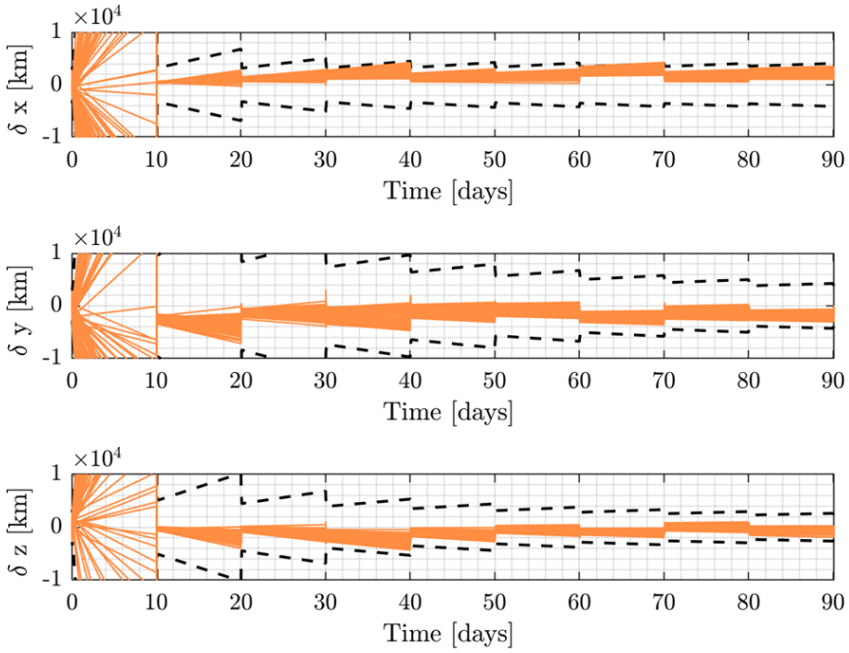

(a) Position

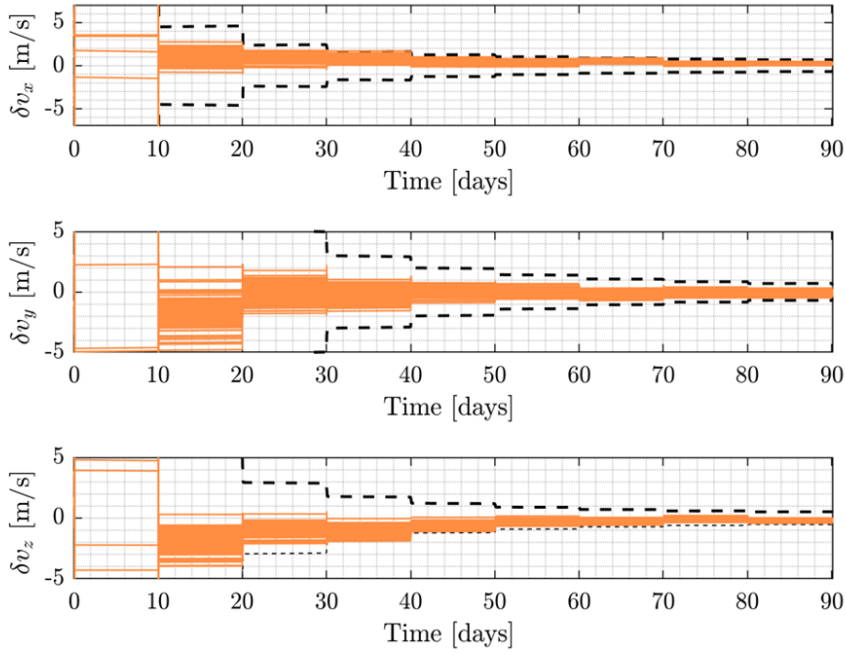

(b) Velocity

Figure 11: Steady-state 3σ errors of the VBN filter in the integrated HIL test.

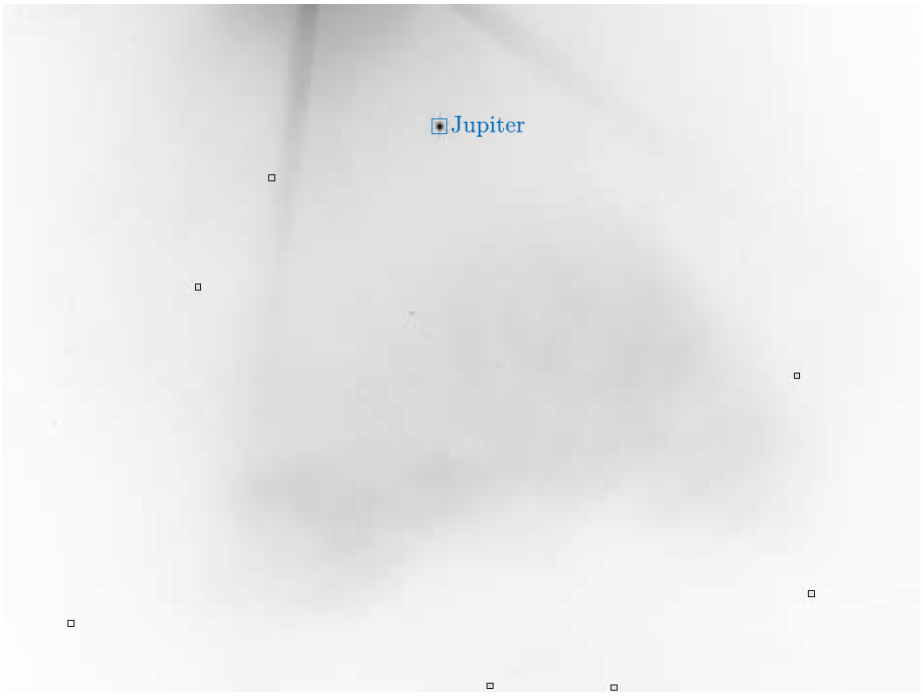

(a) Jupiter

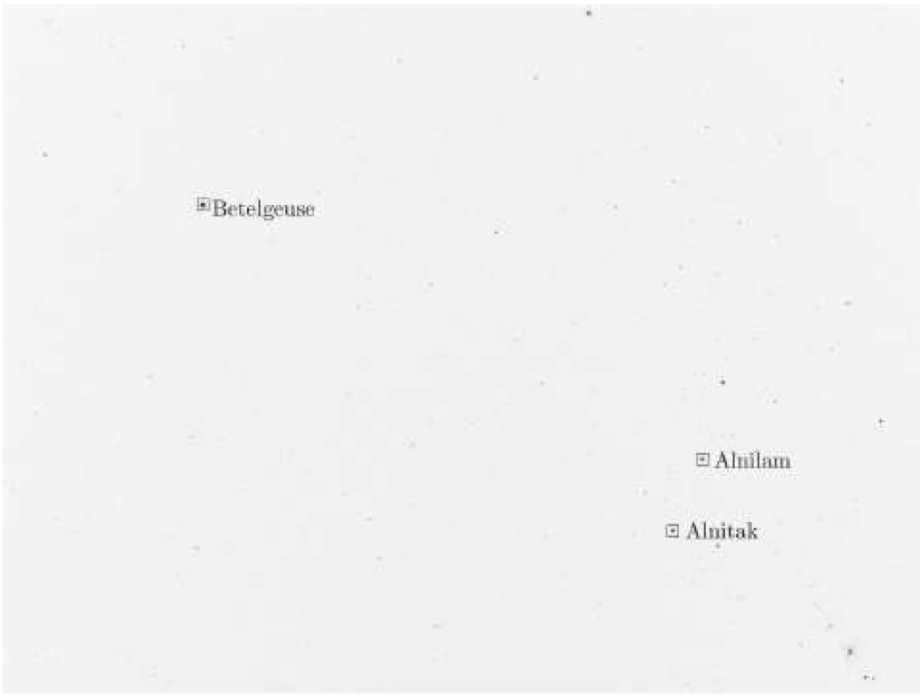

(b) Stars

Figure 12: Representative images from the open-sky validation campaign.

algorithm executing on a space-representative Zynq UltraScale+ SoC. In this configuration, the

pipeline achieved total execution times below 40 ms. Despite the introduction of real hardware and unmodeled effects, the algorithm maintained steady-state position errors below 5,320 km and velocity errors under 1.23 m/s (3σ), demonstrating robust and accurate deep-space navigation. These results provide a comprehensive experimental verification of the system's performance in a relevant environment, confirming that the autonomous navigation algorithm is mature and validated to enable deep space navigation.

ACKNOWLEDGMENT

This research is part of EXTREMA, a project that has received funding from the European Research Council (ERC) under the European Union's Horizon 2020 research and innovation programme (Grant Agreement No. 864697).

REFERENCES

[1] S. Di Pippo, *Space economy: la nuova frontiera dello sviluppo*. EGEA spa, 2022.

[2] A. Poghosyan and A. Golkar, "CubeSat evolution: Analyzing CubeSat capabilities for conducting science missions," *Progress in Aerospace Sciences*, Vol. 88, 2017, pp. 59–83.

[3] R. Walker, D. Binns, C. Bramanti, M. Casasco, P. Concari, D. Izzo, D. Feili, P. Fernandez, J. G. Fernandez, P. Hager, *et al.*, "Deep-space CubeSats: thinking inside the box," *Astronomy & Geophysics*, Vol. 59, No. 5, 2018, pp. 5–24.

[4] C. L. Thornton and J. S. Border, *Radiometric tracking techniques for deep-space navigation*. Wiley Online Library, 2003.

[5] J. A. Starek, B. Açıkmeşe, I. A. Nesnas, and M. Pavone, "Spacecraft autonomy challenges for next-generation space missions," *Advances in control system technology for aerospace applications*, pp. 1–48, Springer, 2015.

[6] A. Malgarini, V. Franzese, and F. Topputo, "Application of pulsar-based navigation for deep-space cubesats," *Aerospace*, Vol. 10, No. 8, 2023, p. 695.

[7] Y. Wang, W. Zheng, S. Sun, and L. Li, "X-ray pulsar-based navigation using time-differenced measurement," *Aerospace Science and Technology*, Vol. 36, 2014, pp. 27–35.

[8] Y. Meng, W. Lei, L. Bian, Y. Wang, T. Yan, and G. Wang, "One-way deep space navigation with radiometric and inertial data fusion," *2017 20th International Conference on Information Fusion (Fusion)*, IEEE, 2017, pp. 1–5.

[9] C. L. Thomton and J. S. Border, "Future Directions in Radiometric Tracking," *Radiometric Tracking Techniques for Deep-Space Navigation*, 2003, p. 63.

[10] L. B. Winternitz, M. A. Hassouneh, J. W. Mitchell, S. R. Price, W. H. Yu, S. R. Semper, P. S. Ray, K. S. Wood, Z. Arzoumanian, and K. C. Gendreau, "SEXTANT X-ray pulsar navigation demonstration: Additional on-orbit results," *2018 SpaceOps conference*, 2018, p. 2538.

[11] S. Bhaskaran, J. Riedel, S. Synnott, and T. Wang, "The Deep Space 1 Autonomous Navigation System-A Post-Flight Analysis," *Astrodynamics Specialist Conference*, AIAA, Denver, CO, USA, August 2000, No. AIAA-2000-3935.

[12] V. Franzese, F. Topputo, F. Ankersen, and R. Walker, "Deep-Space Optical Navigation for M-ARGO Mission," *The Journal of the Astronautical Sciences*, Vol. 68, No. 4, 2021, pp. 1034–1055.

[13] E. Andreis, P. Panicucci, and F. Topputo, "Autonomous Vision-Based Algorithm for Interplanetary Navigation," *Journal of guidance, control, and dynamics*, Vol. 47, No. 9, 2024, pp. 1792–1807.

[14] S. Henry and J. A. Christian, "Absolute Triangulation Algorithms for Space Exploration," *Journal of Guidance, Control, and Dynamics*, Vol. 46, No. 1, 2023, pp. 21–46.

[15] P. Panicucci, J. Lebreton, R. Brochard, E. Zenou, and M. Delpech, "Shadow-Robust Silhouette Reconstruction for Small-Body Applications," *Journal of Spacecraft and Rockets*, Vol. 60, No. 3, 2023, pp. 812–828.

[16] P. Panicucci, J. Lebreton, R. Brochard, E. Zenou, and M. Delpech, "Vision-based estimation of small body rotational state," *Acta Astronautica*, Vol. 213, December 2023, pp. 177–196.

[17] M. Pugliatti, V. Franzese, and F. Topputo, "Data-Driven Image Processing for Onboard Optical Navigation Around a Binary Asteroid," *Journal of Spacecraft and Rockets*, Vol. 59, No. 3, 2022, pp. 943–959.

[18] L. K. McCarthy, C. D. Adam, J. M. Leonard, P. G. Antresian, D. Nelson, E. Sahr, J. Pelgrift, E. J. Lessac-Chenen, J. Geeraert, and D. Lauretta, "OSIRIS-REx Landmark Optical Navigation Performance During Orbital and Close Proximity Operations at Asteroid Bennu," *AIAA SCITECH 2022 Forum*, January 2022.

[19] B. Maass, S. Woicke, W. M. Oliveira, B. Razgus, and H. Krüger, "Crater Navigation System for Autonomous Precision Landing on the Moon," *Journal of Guidance, Control, and Dynamics*, Vol. 43, No. 8, 2020, pp. 1414–1431.

[20] P. Califano, F. Piccolo, P. Panicucci, F. Topputo, *et al.*, "Enhanced Full Visual Slam for Close Proximity Exploration of Asteroids Combining Incremental Smoothing with Filtering Techniques," *35th AAS/AIAA Space Flight Mechanics Meeting*, 2025, pp. 1–22.
[21] E. Andreis, V. Franzese, and F. Topputo, "Onboard Orbit Determination for Deep-Space CubeSats," *Journal of Guidance, Control, and Dynamics*, Vol. 45, No. 8, 2022, pp. 1466–1480.
[22] R. Raymond Karimi and D. Mortari, "Interplanetary autonomous navigation using visible planets," *Journal of Guidance, Control, and Dynamics*, Vol. 38, No. 6, 2015, pp. 1151–1156.
[23] P. Lu, "GN&C Algorithm Verification and Validation," 2025.
[24] S. Bennani, B. Girouart, M. Casasco, D. Oddenino, J. Vandersteen, G. Constant-Filaire, S. Delavault, H. Evain, M. Morere, J.-M. Biannic, *et al.*, "Looking to the Future: A Call to Action for Advanced GNC Algorithm Verification and Validation," 2024.
[25] P. Panicucci, C. Balossi, F. Ornati, F. Piccolo, A. Pizzetti, F. Topputo, F. Capolupo, *et al.*, "What if Star Trackers Were Navigation Cameras?," *35th AAS/AIAA Space Flight Mechanics Meeting*, 2025, pp. 1–23.
[26] F. Ornati, P. Panicucci, A. Pizzetti, F. Capolupo, and F. Topputo, "On the radiometric calibration of optical Hardware-In-the-Loop stimulators," *Journal of Spacecraft and Rockets*, 2026.
[27] G. Di Domenico, E. Andreis, A. Carlo Morelli, G. Merisio, V. Franzese, C. Giordano, A. Morselli, P. Panicucci, F. Ferrari, and F. Topputo, "The erc-funded extrema project: Achieving self-driving interplanetary cubesats," *Modeling and Optimization in Space Engineering: New Concepts and Approaches*, pp. 167–199, Springer, 2022.
[28] P. Panicucci and F. Topputo, "The tinyv3rse hardware-in-the-loop vision-based navigation facility," *Sensors*, Vol. 22, No. 23, 2022, p. 9333.
[29] P. Panicucci, F. Ornati, and F. Topputo, "Design of a Low-Aberration Variable-Magnification Optical Stimulator for Vision System Hardware-in-The-Loop Testing," *IEEE Transactions on Aerospace and Electronic Systems*, 2025.
[30] A. Pizzetti, P. Panicucci, F. Capolupo, and F. Topputo, "Development and Validation of a Physically Based Rendering Methodology for Celestial Bodies," *Acta Astronautica*, 2025. Under review.
[31] F. Gallet, C. Marabotto, and T. Chambon, "Exploring AI-Based Satellite Pose Estimation: from Novel Synthetic Dataset to In-Depth Performance Evaluation," *Proceedings of the IEEE/CVF Conference on Computer Vision and Pattern Recognition (CVPR) Workshops*, June 2024, pp. 6770–6778.
[32] J. Lebreton, R. Brochard, M. Baudry, G. Jonniaux, A. H. Salah, K. Kanani, M. L. Goff, A. Masson, N. Ollagnier, P. Panicucci, *et al.*, "Image simulation for space applications with the SurRender software," *arXiv preprint arXiv:2106.11322*, 2021.
[33] I. Martin, M. Dunstan, and M. S. Gestido, "Planetary surface image generation for testing future space missions with pangu," *2nd RPI Space Imaging Workshop*, Sensing, Estimation, and Automation Laboratory, 2019.
[34] C. Giordano, F. Topputo, *et al.*, "Spesi: A real-time space environment simulator for the extrema project," *33rd AAS/AIAA Space Flight Mechanics Meeting*, 2023, pp. 1–13.
[35] M. A. Perryman, L. Lindegren, J. Kovalevsky, E. Hoeg, U. Bastian, P. Bernacca, M. Crézé, F. Donati, M. Grenon, M. Grewing, *et al.*, "The HIPPARCOS catalogue," *Astronomy and Astrophysics, Vol. 323, p. L49-L52*, Vol. 323, 1997, pp. L49–L52.
[36] E. Høg, "Tycho Star Catalogs: The 2.5 Million Brightest Stars," *Encyclopedia of Astronomy & Astrophysics*, pp. 1–3, CRC Press, 2001.
[37] G. Muller, "Number 30. Achten Bandes Viertes Stuck. Helligkeitsbestimmungen der grossen planeten und einiger asteroiden.," *Publikationen des Astrophysikalischen Observatoriums zu Potsdam, Vol. 8, p. 193-389*, Vol. 8, 1893, pp. 193–389.
[38] A. Mallama and J. L. Hilton, "Computing apparent planetary magnitudes for The Astronomical Almanac," *Astronomy and computing*, Vol. 25, 2018, pp. 10–24.
[39] M. D. Shuster, "Stellar Aberration and Parallax: A Tutorial," *The Journal of the astronautical sciences*, Vol. 51, August 2003, pp. 477–494.
[40] A. Eleonora, "Autonomous Vision-Based Navigation for Deep-Space CubeSats: Algorithmì Development and Hardware Validation," 2024.
[41] K.-H. Glassmeier, H. Boehnhardt, D. Koschny, E. Kührt, and I. Richter, "The Rosetta mission: flying towards the origin of the solar system," *Space Science Reviews*, Vol. 128, No. 1, 2007, pp. 1–21.
[42] B. Geiger, R. Andrés, and T. Statella, "Radiometric Calibration of the Rosetta Navigation Camera," *Journal of Astronomical Instrumentation*, Vol. 10, No. 01, 2021, p. 2150004.
[43] V. Franzese and F. Topputo, "Optimal beacons selection for deep-space optical navigation," *The Journal of the Astronautical Sciences*, Vol. 67, No. 4, 2020, pp. 1775–1792.
[44] V. Franzese and F. Topputo, "Celestial bodies far-range detection with deep-space CubeSats," *Sensors*, Vol. 23, No. 9, 2023, p. 4544.
[45] E. Andreis, P. Panicucci, V. Franzese, and F. Topputo, "A Robust Image Processing Pipeline for Planets Line-Of-Sight Extraction for Deep-Space Autonomous Cubesats Navigation," *Proceedings of the 44th Annual American Astronautical Society Guidance, Navigation, and Control Conference, 2022*, Springer, 2024, pp. 1103–1121.

[46] X. Wan, G. Wang, X. Wei, J. Li, and G. Zhang, "Star centroiding based on fast Gaussian fitting for star sensors," *Sensors*, Vol. 18, No. 9, 2018, p. 2836.
[47] D. Mortari, M. A. Samaan, C. Bruccoleri, and J. L. Junkins, "The pyramid star identification technique," *Navigation*, Vol. 51, No. 3, 2004, pp. 171–183.
[48] C. Beierle, J. Sullivan, and S. D'amico, "High-fidelity verification of vision-based sensors for inertial and far-range spaceborne navigation," *26th International Symposium on Space Flight Dynamics (ISSFD)*, 2017.
[49] C. Beierle and S. D'Amico, "Variable-magnification optical stimulator for training and validation of spaceborne vision-based navigation," *Journal of Spacecraft and Rockets*, Vol. 56, No. 4, 2019, pp. 1060–1072.